A π-d Conjugated Metal-Organic Framework Decorated on MXene-Carbon Nanofiber as a Self-Standing Electrode for Flexible Supercapacitors

Zahir Abbas [a] and Shaikh M. Mobin [a, b*]

[a] Department of Chemistry, Indian Institute of Technology Indore, Simrol, Khandwa Road, Indore, 453552, India.

[b] Centre for Advanced Electronics (CAE), Indian Institute of Technology Indore, Simrol, Khandwa Road, Indore 453552, India.

*Email: xray@iiti.ac.in

1. Materials and Methods

1.1 Materials

Titanium aluminum carbide was purchased from Otto Chemie, Nickel chloride hexahydrate ($NiCl_2 \cdot 6H_2O$), Dimethyl formamide (DMF), and Methanol, tetrahydrofuran, and trimethylamine Potassium hydroxide (KOH) were purchased from SRL chemicals. Ammonia solutions were purchased from spectrochem. Lithium fluoride was purchased from SRL chemicals and Ni foam and activated carbon were purchased from Global Nanotech Pvt. Ltd. Deionized water (DI) was used throughout the study. All the chemicals used as received without further purification. Benzene 1, 2, 4, and 5 tetramine tetra hydrochloride ligand was purchased from Sigma Aldrich.

1.2 Characterizations

All the reagents and solvents were purchased from a commercial source without any further purification. For the Powder X-ray diffraction (PXRD) analysis, Cu Kα (0.154 nm) monochromatic radiation was used with a Rigaku Smart Lab X-ray diffractometer. The morphologies were investigated by a Supra55 Zeiss field emission scanning electron microscope (FESEM) and high-resolution transmission electron microscopy (HR-TEM) was performed using (TEM, JEM F200). Brunauer−Emmett−Teller (BET) surface area and Barrett−Joyner−Halenda (BJH) distribution determinations were conducted on an Autosorb iQ (Quantachrome Instruments, version 1.11). X-ray photoelectron spectroscopic (XPS) analysis (XPS, Nexsa, Thermofisher Scientific) incorporating Al Kα as the source of X-ray.

1.3 Synthesis of π-d c-MOF

c-MOF was synthesized generally at low-temperature synthesis. In this work π-d c-MOF via coordination polymerization reaction at room temperature. Initially, 0.2 mmol of 1,2,4,5-benzene tetramine (BTA·4HCl) was dissolved in 5 ml DI water and stirred until complete dissolution as solution A. Then 0.2 mmol of $NiCl_2 . 6H_2O$ was dissolved in another 5ml DI water as solution B. Solution B was slowly added to solution A to get a dark purple mixture. Then 0.5 ml of ammonia solution was added and stirred for 10 h at room temperature to get a light brown powder, it was washed with water, and acetone and then dried at 50℃. The synthesis of this MOF was carried out by following the protocol from the literature.[1]

1.4 Electrochemical measurement in a three-electrode system

Electrochemical measurement in a three-electrode system was studied at room temperature. The prepared c-MOF@MX-CNF freestanding electrode was carefully cut into 1 × 2 cm^2 approximately mass loading (2 to 3 mg) used as a working electrode with Ag/AgCl as a reference electrode, and platinum wire as the counter electrode in three electrodes set up. To determine the electrochemical performance, cyclic voltammetry (CV), galvanostatic charge-discharge (GCD) curve measurements, and electrochemical impedance spectroscopy (EIS) were carried out on an Autolab workstation using a 2 M KOH aqueous solution as an electrolyte. The efficiency evaluation was determined by the following equations summarised. The electrochemical study of control samples i.e., 2 mg pristine c-MOF dispersed in ethanol and drop cast on Ni foam used as the working electrode.

1.5 Gel preparation and Device fabrications

The two-electrode system was fabricated using carbon cloth as the current collector. As for the electrolytes, PVA–KOH was applied to the electrodes. PVA (1 g) was added to H_2O (10 mL) at 90 °C to produce a transparent solution. Subsequently, 3.0 g of KOH in 10 mL of water was added with full agitation until the PVA aqueous solution cooled to room temperature. Finally, PVA–KOH gel was coated on the electrode, which was solidified at room temperature. Finally, the assembly of the solid-state supercapacitor demonstrated that the positive electrode (c-MOF@MX-CNF) and negative electrode (AC) were completely separated by cellulose paper and fixed for further use to record the efficiency of the devices.

1.6 Efficiency Calculations

The specific capacitance of as-synthesized electrode materials was evaluated through the GCD curves by using the following relation.[2]

$$Cs = \frac{I \times \Delta t}{m \times \Delta V} \qquad 1$$

where I/m, Δt, and ΔV represent current density, discharge time, and the potential range of the GCD profile, respectively.

Furthermore, the energy density (E) and power density (P) of the asymmetric device (ASC) were calculated by the following relations

$$E = \frac{Cs}{2 \times 3.6}\Delta V^2 \qquad 2$$

$$P = \frac{E}{\Delta t} \times 3600 \qquad 3$$

where C_s, ΔV, and Δt indicate the specific capacitance, potential window, and discharge time of the GCD profile, respectively.

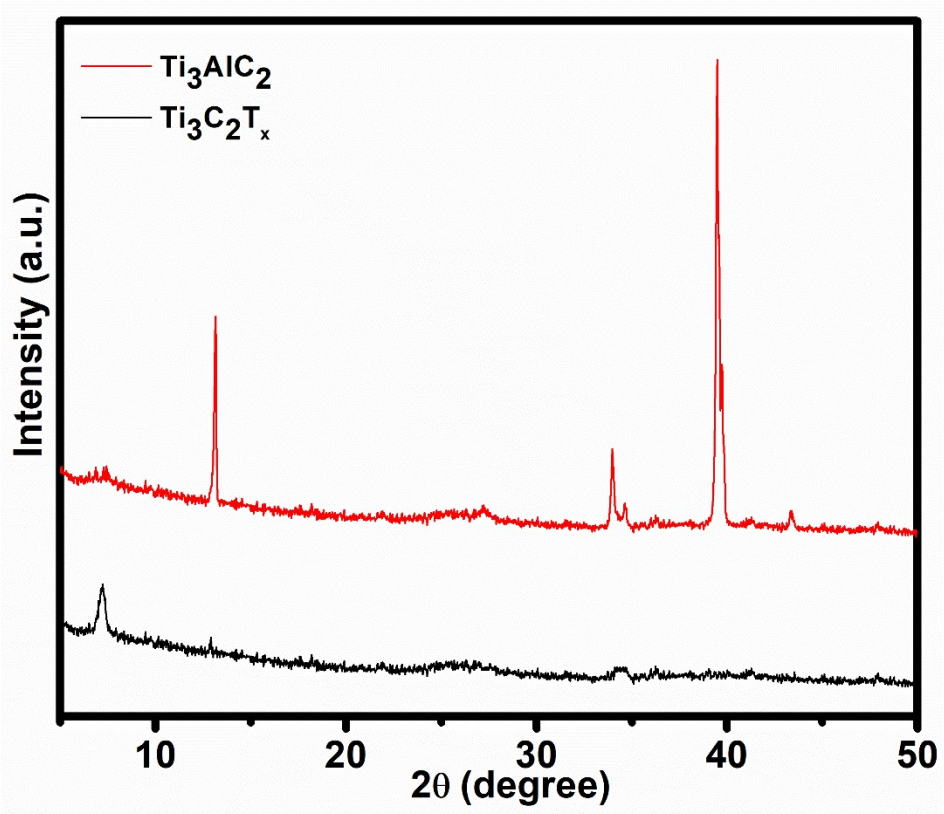

Fig. S1. PXRD pattern of Ti_3C_2Tx MXene along with Ti_3AlC_2.

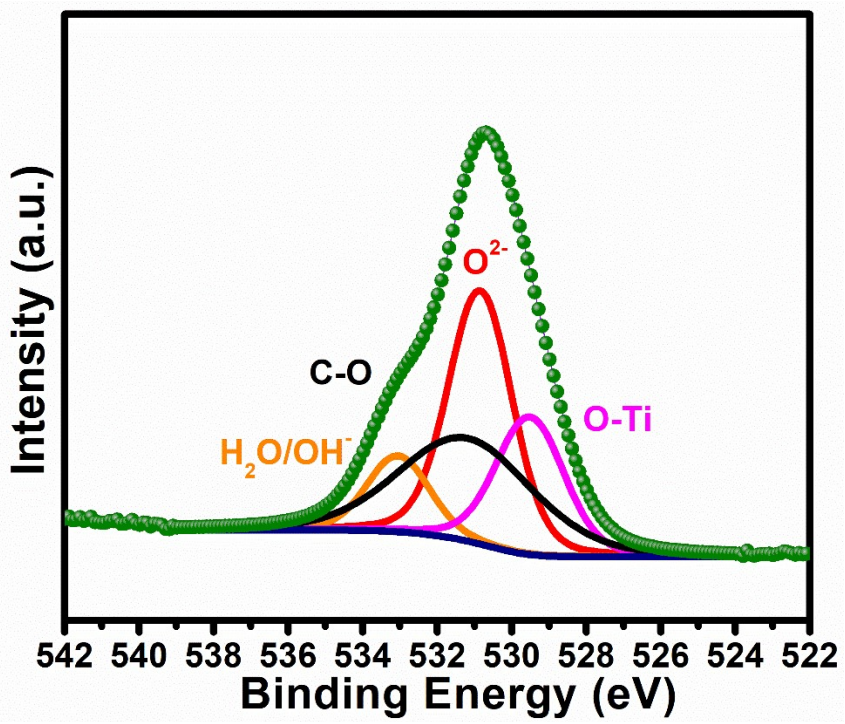

Fig S2. XPS deconvoluted spectra of O 1s, c-MOF@MX-CNF.

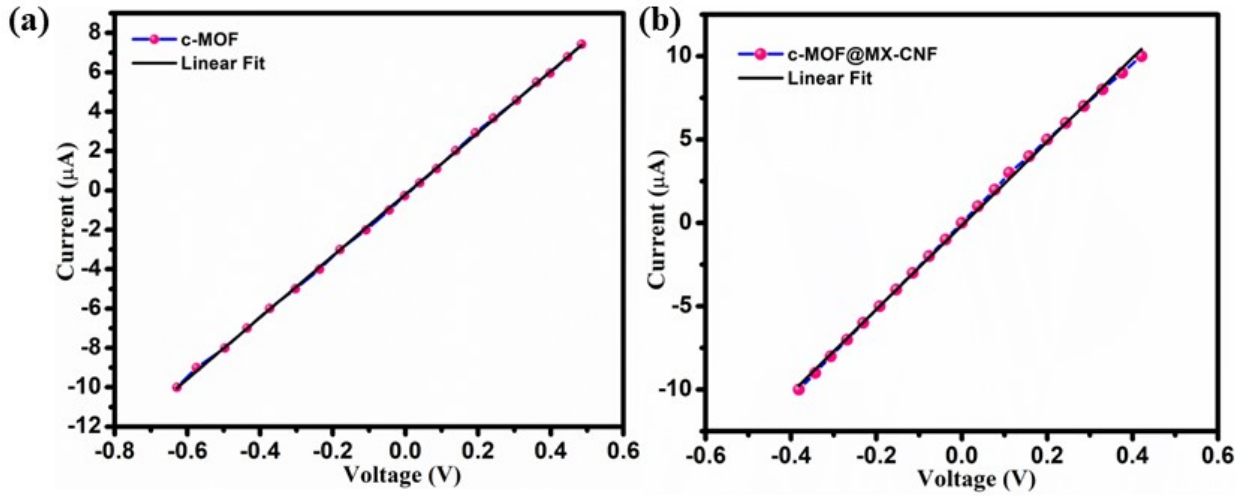

Fig. S3. Electrical conductivity measurements: Current (I) *vs* voltage (V) plot for (a) c-MOF and (b) c-MOF@MX-CNF.

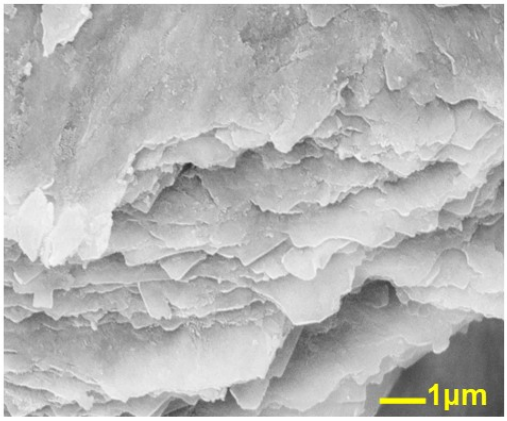

Fig. S4. SEM image of Ti_3C_2Tx MXene.

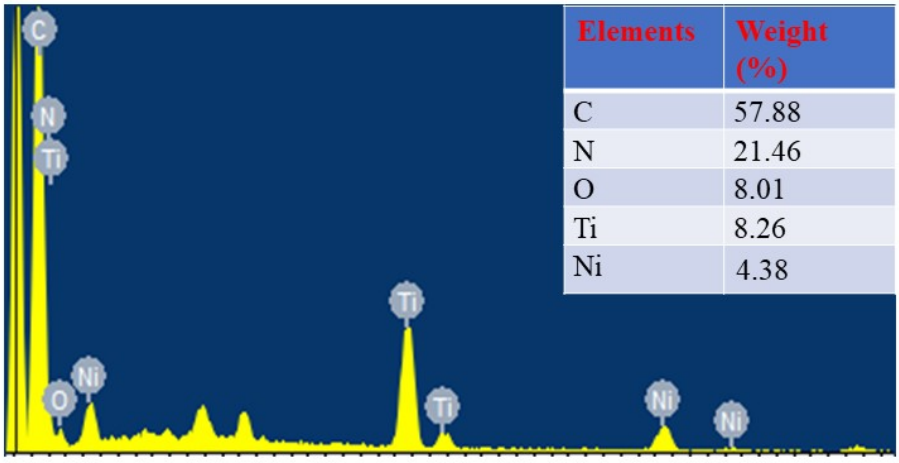

Elements	Weight (%)
C	57.88
N	21.46
O	8.01
Ti	8.26
Ni	4.38

Fig. S5. EDX elemental analysis of c-MOF@MX-CNF.

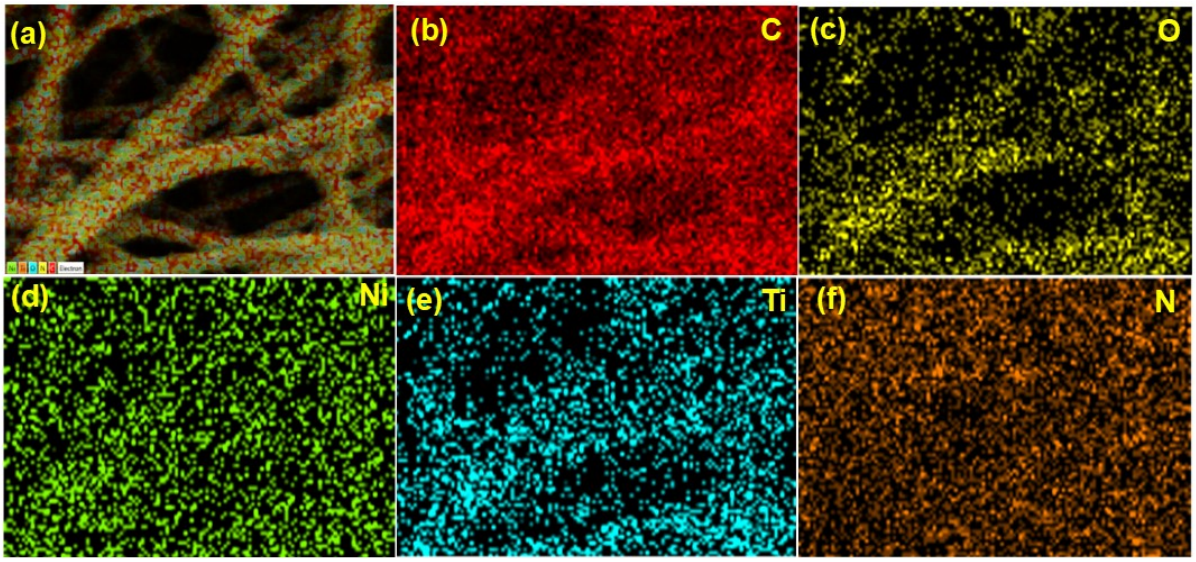

Fig. S6. (a) Electron image of c-MOF@MX-CNF and EDS elemental mapping of c-MOF@MX-CNF (b) C (c) O (d) Ni (e) Ti (f) N.

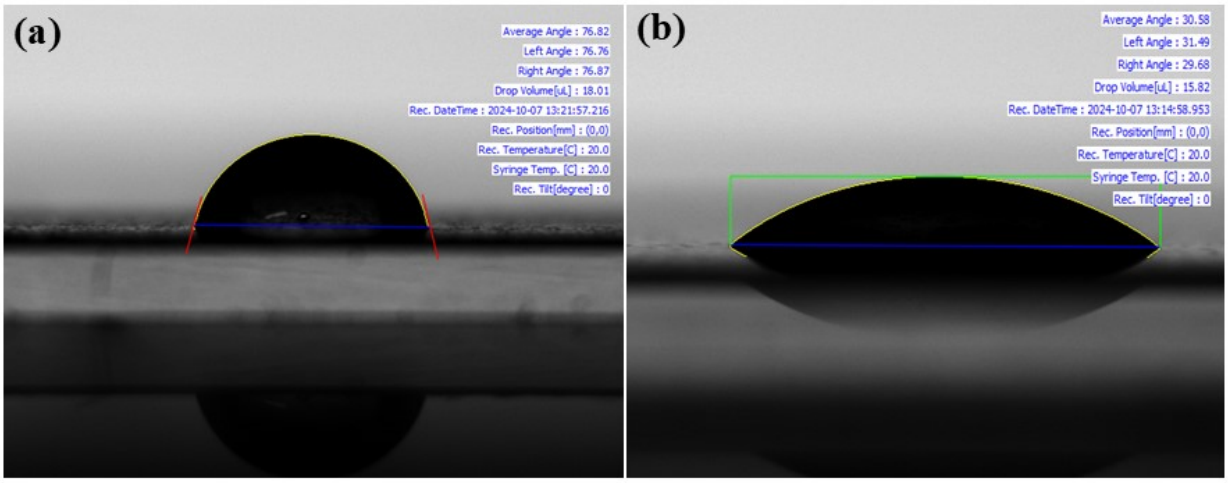

Fig. S7. Water Contact angle measurement of (a) CNF is 76.82˚ (b) MX-CNF is 30.58˚.

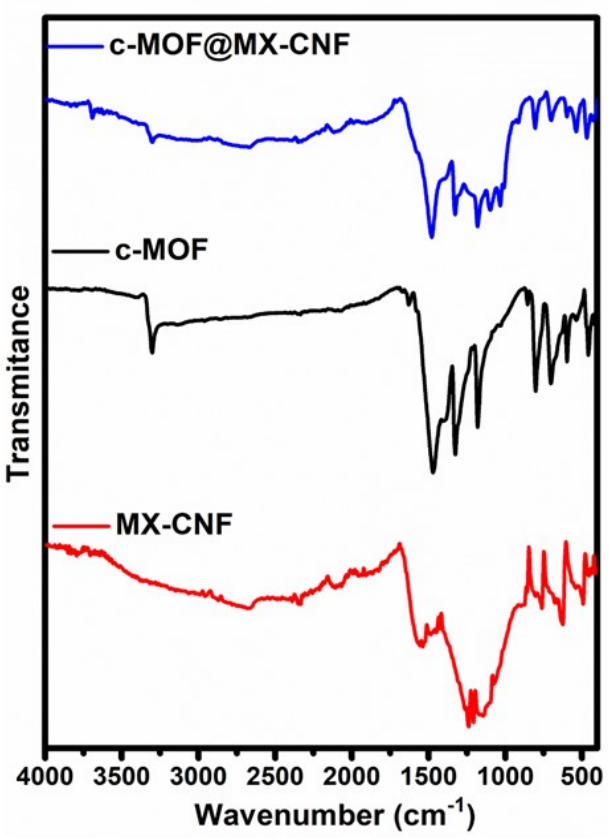

Fig. S8. FTIR analysis of c-MOF, MX-CNF, and c-MOF@MX-CNF.

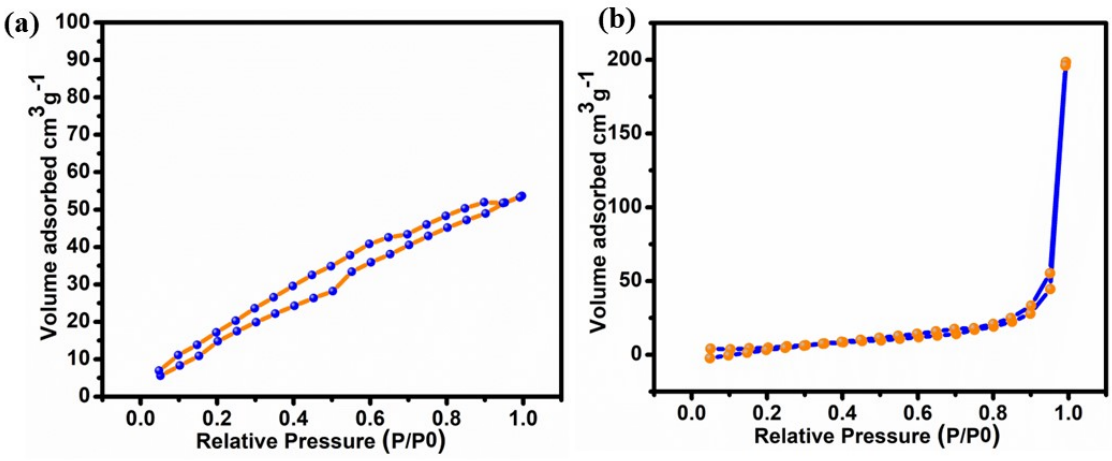

Fig. S9. (a) BET plot of MX-CNF (b) BET plot of c-MOF@MX-CNF.

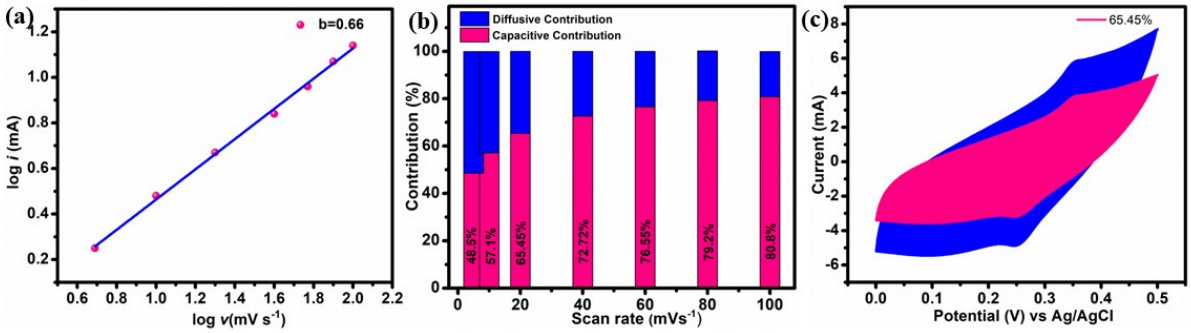

Fig.S10: (a) Log *i* (peak current) versus log *v* (scan rate) plots obtained from CV data. (b) Capacitive contributions at various CV scan rates. (c) CV curve with a capacitive contribution at 20 mV s^{-1}.

The charge storage mechanism and reaction kinetics of c-MOF@MX-CNF were examined in more detail using the power law, as illustrated in equ. 4.[3,4]

$$I_p = av^b \qquad 4$$

I_p stands for the peak current, v denotes the scan rate, and a and b are the changeable parameters in this case. The following equation 5, as illustrated in, states that the "b" value is estimated using the slope of the linear fit graph log(Ip) v/s log(v).[5]

$$\log I = \log a + b \log v \qquad 5$$

Where *I* denote the peak current at a constant potential, v stands for scan rate in the CV curve, and a and b are variable parameters. Whereas b = 1.0 for a capacitive-controlled process with a surface diffusion process, and b = 0.5 for electrode materials with diffusion-controlled behavior. The plot of log(i) versus log(v) to get the b value, as shown in **Fig. S10a.** It illustrates the resulting slope was 0.66. Therefore, it is evident from the obtained b value that capacitive-controlled behavior is the source of the charge storage mechanism. Moreover, the following equations were used to analyze the specific analysis contribution of the surface-controlled and diffusion-controlled processes in the c-MOF@MX-CNF electrode material at a certain scan rate.

$$i(v) = k_1 v + k_2 v^{1/2} \qquad 6$$

$$i/v^{1/2} = k_1 v^{1/2} + k_2 \qquad 7$$

where $k_2v^{1/2}$ is diffusion controlled and k_1v is surface or capacitive regulated (EDLC and pseudocapacitance), and i and v are current and scan rates, respectively. Additionally, the contribution from the diffusion- and surface-controlled processes was computed at various scan rates, ranging from 5 mV s^{-1} to 100 mV s^{-1}. It was evident that when the scan rate rises, the diffusion contribution was reduced, and the capacitive contribution increased. Nevertheless, the c-MOF@MX-CNF electrode demonstrated a 48.5% capacitive contribution at 5 mV s^{-1}, an 80.8% capacitive contribution at 100 mV s^{-1}, and a markedly improved capacitance behavior for a quick charge storage procedure as depicted in **Fig. S10b.** The contributions of the c-MOF@MX-CNF electrode's diffusion-controlled charge and surface-capacitive charge are shown by the blue-shaded area (34.55%) and pink-shaded area (65.45%). This value is near the b = 0.66 slope value (**Fig. S10c**). The capacitive-controlled percentage was expected to be 48% at a lower scan rate of 5 mV s^{-1}, demonstrating the viability of electrolyte ion insertion and the dominating diffusion-controlled mechanism. Diffusion-controlled contribution current reduced at high scan rates. This is a result of the redox processes between the electrolyte and electrode active materials becoming insufficient at higher scan rates. However, it is challenging to intercalate OH^- ions into the electrode at higher scan rates.

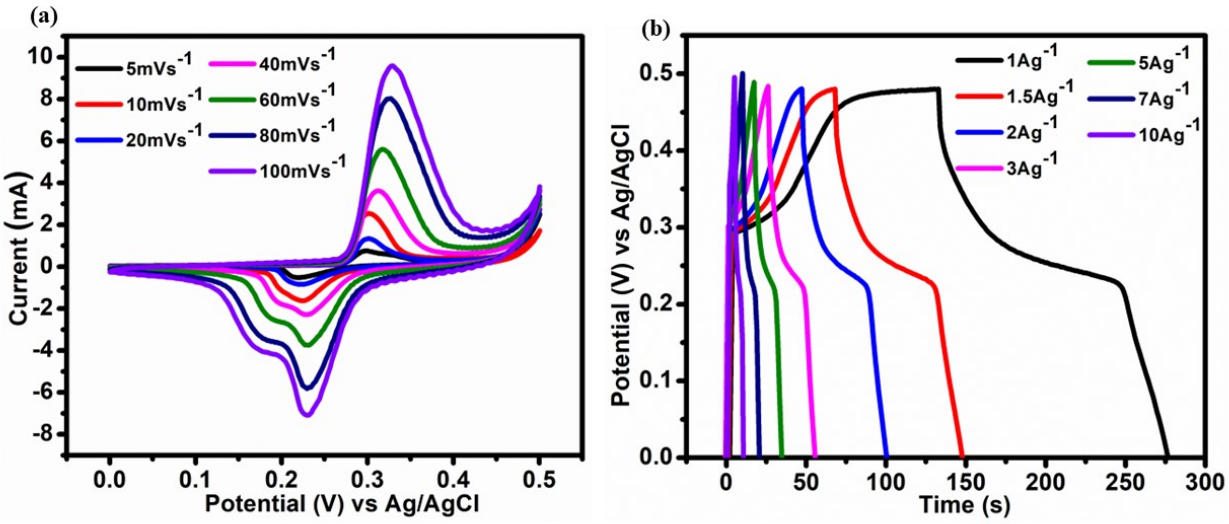

Fig. S11. (a) Cyclic voltammetry curve of c-MOF (b) GCD curve of c-MOF.

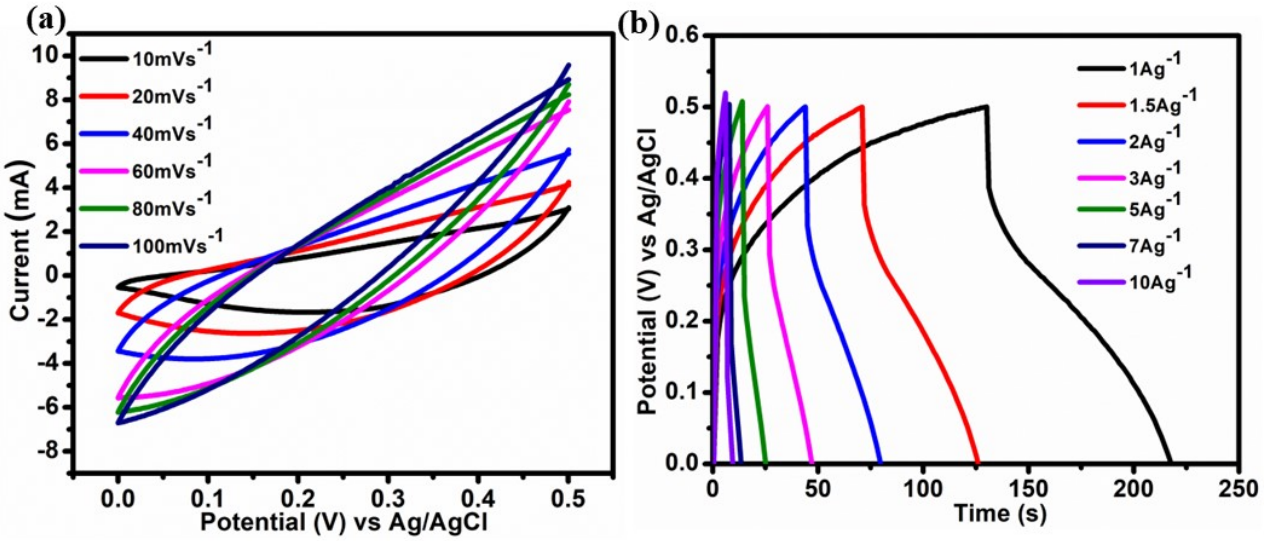

Fig. S12. (a) Cyclic voltammetry curve of MX-CNF (b) GCD curve of MX-CNF.

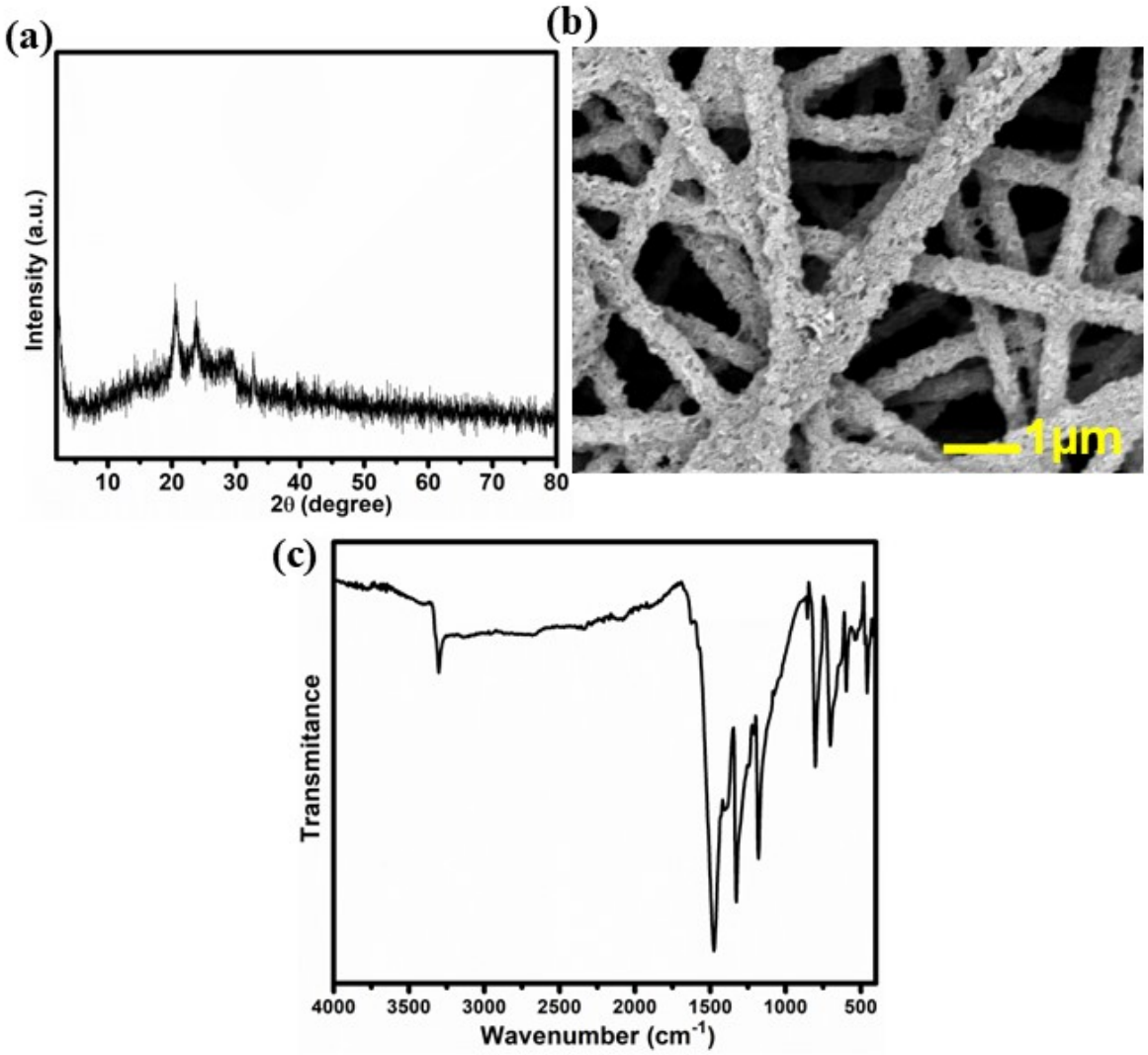

Fig. S13. Post electrochemical characterization of c-MOF@MX-CNF (a) PXRD analysis (b) SEM analysis (c) FT-IR spectrum.

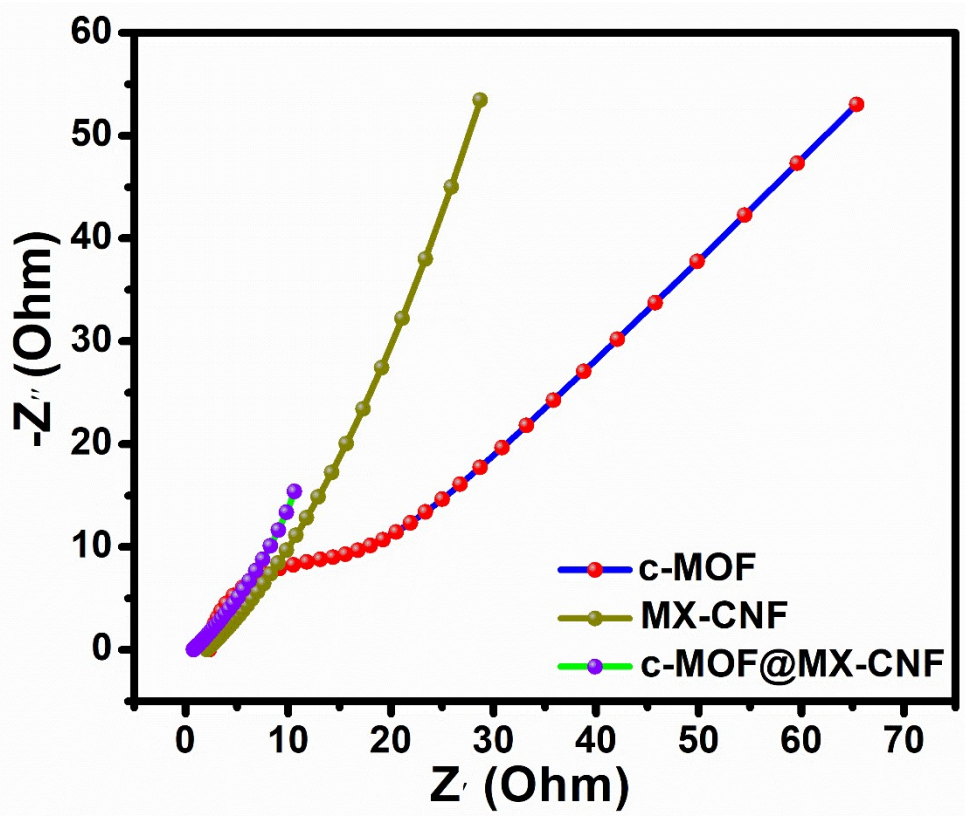

Fig. S14. EIS plot of c-MOF, MX-CNF, and c-MOF@MX-CNF.

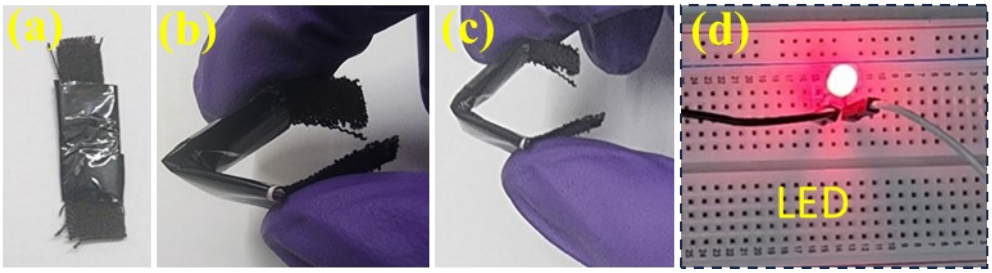

Fig. S15. Device Photographs (a) Flat (b-c) with different bending modes and (d) enlightened LED.

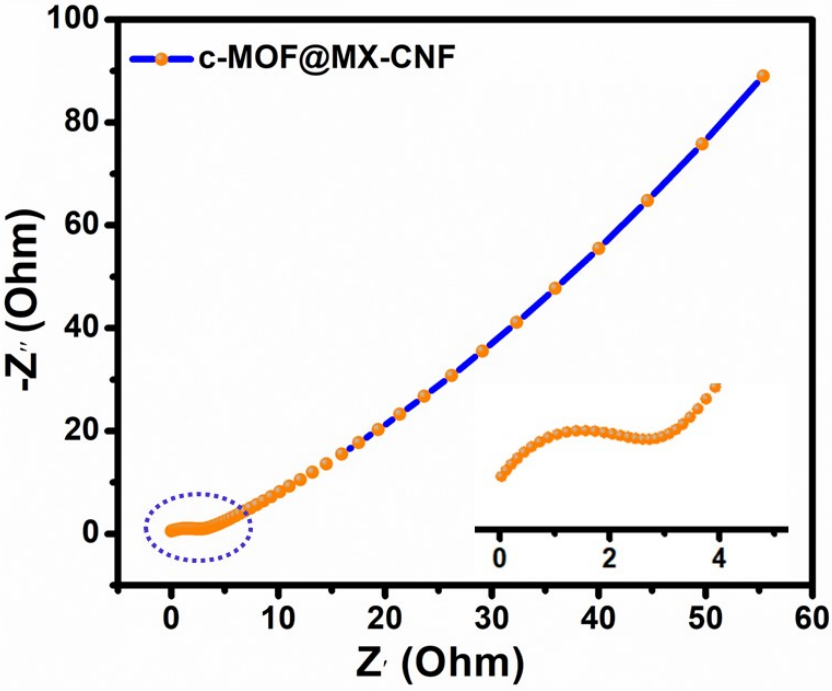

Fig. S16. EIS plot of c-MOF@MX-CNF//AC ASC device.

Table. S1 Comparison of electrochemical performance of redox-active c-MOF@MX-CNF with the previously reported MOF and MXene nanofiber-based electrode.

S. No.	**Electrode materials**	**Specific capacitance/ Capacity (Fg^{-1})/ (Cg^{-1})**	**Current density (Ag^{-1})/ 2 mV/s**	**Cycling stability**	**Ref.**
1	Co-MOF@MXene nanofiber derived Co-PC@MX-CNF	426.7 Fg^{-1}	1 Ag^{-1}	90.36% after 10,000 Cycles	[6]
2	MOF@CNF derived Co–S@CNF–CNT-3	416.6 Fg^{-1}	0.2 Ag^{-1}	96.6% after 10,000 Cycles	[7]
3	CNF@Ni-CAT MOF	502.95 Fg^{-1}	0.5 Ag^{-1}	73% after 10,000 Cycles	[8]
4.	MnO_2@$Ti_3C_2T_x$/CNFs	462.8 Fg^{-1}	1 Ag^{-1}	81% after 5000 cycles	[9]
5	$Ti_3C_2T_x$ MXene/carbon nanofibers-RuOx	279.4 F/g	2 mV/s	99% after 10,000 Cycles	[10]
6	FOCNF NOCNF	523 Fg^{-1} 468 Fg^{-1}	1 Ag^{-1} 1 Ag^{-1}	81.3% after 10,000 Cycles	[11]
7	PAN/ZIF-based HPCNFs	307.2 Fg^{-1}	1 Ag^{-1}	98.2% after 10,000 Cycles	[12]
8	Cu-MOF@ACNF	303 Fg^{-1}	1 Ag^{-1}	-	[13]
9	MOF/MXene nanofiber derived MX-5@PCNF	572 Fg^{-1}	1 Ag^{-1}	71.24% after 10,000 Cycles	[14]
10	**c-MOF@MX-CNF**	**1076 Fg^{-1}**	**1 Ag^{-1}**	**86.4% after 15,000 cycles**	**This Work**

References

1Z. Sang, J. Liu, X. Zhang, L. Yin, F. Hou and J. Liang, *ACS Nano*, 2023, **17**, 3077–3087.

2D. Tian, N. Song, M. Zhong, X. Lu and C. Wang, *ACS Appl. Mater. Interfaces*, 2020, **12**, 1280–1291.

3Q. Yang, Q. Wang, Y. Long, F. Wang, L. Wu, J. Pan, J. Han, Y. Lei, W. Shi and S. Song, *Advanced Energy Materials*, 2020, **10**, 1903193.

4B. Long, M.-S. Balogun, L. Luo, W. Qiu, Y. Luo, S. Song and Y. Tong, *Advanced Energy Materials*, 2018, **8**, 1701681.

5H. Fu, A. Zhang, H. Guo, L. Duan, F. Jin, H. Zong, X. Sun and J. Liu, *ACS Appl. Mater. Interfaces*, 2023, **15**, 8169–8180.

6T. Kshetri, D. D. Khumujam, T. I. Singh, Y. S. Lee, N. H. Kim and J. H. Lee, *Chemical Engineering Journal*, 2022, **437**, 135338.

7M. Yao, C. Guo, Y. Zhang, X. Zhao and Y. Wang, *Journal of Materials Chemistry C*, 2022, **10**, 542–548.

8S. Zhao, H. Wu, Y. Li, Q. Li, J. Zhou, X. Yu, H. Chen, K. Tao and L. Han, *Inorg. Chem. Front.*, 2019, **6**, 1824–1830.

9Z. Wang, D. Zhang, Y. Guo, H. Jiang, D. Wang, J. Cheng, P. K. Chu, H. Yan and Y. Luo, *Chem. Commun.*, 2023, **59**, 14309–14312.

10 H. Hwang, S. Yang, S. Yuk, K.-S. Lee, S. Byun and D. Lee, *NPG Asia Mater*, 2023, **15**, 1–13.

11 Y. Li, G. Zhu, X. Xu, L. Chen, T. Lu, J. P. Hill, L. Pan and Y. Yamauchi, *Small Structures*, 2022, **3**, 2200015.

12 L.-F. Chen, Y. Lu, L. Yu and X. W. (David) Lou, *Energy Environ. Sci.*, 2017, **10**, 1777–1783.

13 M. Singh, A. Gupta, P. Saharan, C. Kumar, S. Sundriyal, R. Padhye, T. Daeneke, N. R. Choudhary and S. R. Dhakate, *Journal of Energy Storage*, 2023, **67**, 107617.

14 I. Pathak, D. Acharya, K. Chhetri, P. C. Lohani, S. Subedi, A. Muthurasu, T. Kim, T. H. Ko, B. Dahal and H. Y. Kim, *J. Mater. Chem. A*, 2023, **11**, 5001–5014.